

A Fully Digital Relaxation-Aware Analog Programming Technique for HfO_x RRAM Arrays

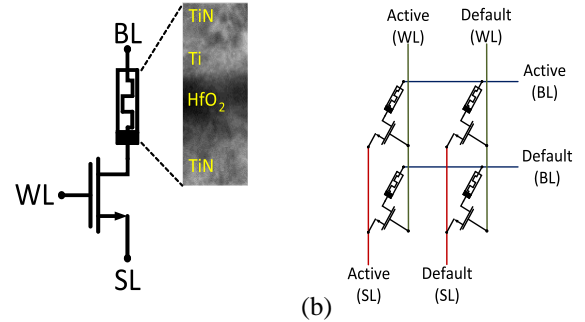
Hamidreza Erfanijazi, Luis A. Camuñas-Mesa, Elisa Vianello, Teresa Serrano-Gotarredona *Senior Member, IEEE*, and Bernabé Linares-Barranco, *Fellow, IEEE*

Abstract— For neuromorphic engineering to emulate the human brain, improving memory density with low power consumption is an indispensable but challenging goal. In this regard, emerging RRAMs have attracted considerable interest for their unique qualities like low power consumption, high integration potential, durability, and CMOS compatibility. Using RRAMs to imitate the more analog storage behavior of brain synapses is also a promising strategy for further improving memory density and power efficiency. However, RRAM devices display strong stochastic behavior, together with relaxation effects, making it more challenging to precisely control their multi-level storage capability. To address this, researchers have reported different multi-level programming strategies, mostly involving the precise control of analog parameters like compliance current during write operations and/or programming voltage amplitudes. Here, we present a new fully digital relaxation-aware method for tuning the conductance of analog RRAMs. The method is based on modulating digital pulse widths during erase operations while keeping other parameters fixed, and therefore requires no precise alterations to analog parameters like compliance currents or programming voltage amplitudes. Experimental results, with and without relaxation effect awareness, on a 64 RRAM 1T1R HfO_x memory array of cells, fabricated in 130nm CMOS technology, indicate that it is possible to obtain 2-bit memory per cell multi-value storage at the array level, verified 1000 seconds after programming.

Index Terms— Analog RRAM, Multi-Level RRAM, Pulse width modulation, Conductive states, Memristive crossbar, Relaxation and retention effects, Neuromorphic applications.

I. INTRODUCTION

HfO_x-based Resistive Random Access Memory (RRAM) technology is promising for implementing low-power non-volatile, compact but computationally-efficient CMOS-compatible neuromorphic edge devices. RRAM devices can be used to emulate the synaptic knowledge-storage devices in the brain which, being connected between neurons, also directly participate in computing processes, overcoming the memory-wall power problem of Von-Neumann-based computing systems [1]. This efficiency can be further boosted if RRAM devices can store multi-level values. For example, brain synapses have been shown to be capable of storing 26 different weights each (4.7 bits per synapse) [2]. In practice, however, RRAM devices suffer from considerable device-to-device and cycle-to-cycle variability, as well as short-term and long-term stochastic degradation effects, and are therefore mainly used reliably as binary (2-state) memory devices (1 bit per synapse) [3]. Nonetheless, some techniques have been



(a) Schematic diagram of a 1T1R memory (synaptic) element composed of one NMOS transistor and one RRAM TiN/Ti/HfO₂/TiN device, controlled by three terminal voltages: one word-line (WL), one bit-line (BL), and one source-line (SL). (b) Simplified representation of a 1T1R crossbar: the “Default” column and row lines represent multiples sharing the same terminal (WL, BL, SL) voltages, while there are only one “Active” (WL, SL) column and line (BL) selecting one single 1T1R memory device.

reported recently which are capable of successfully achieving multi-level storage per individual RRAM device in monolithically fabricated CMOS+RRAM crossbar 1T1R arrays (see Fig. 1). The reported techniques typically require iterative write/erase steps per device by gradually precision tuning a given analog parameter per each 1T1R device. Some researchers, for example, report having achieved successful 4-level post-relaxation storage by careful iterative tuning of the analog compliance current at each write operation [4]-[9]. Another technique consists of progressively changing analog write and/or erase voltage pulse amplitudes [10]-[13]. The added problem of stochastic degradation of the analog programmed value seems to comprise two components: (a) a fast sub-5-second and stronger short-term relaxation, and (b) a slower minute-range but weaker long-term retention loss [11]. To mitigate these effects, Esmanhotto et al. [5] proposed introducing a 5-second waiting step at device level before every read verification after each programming attempt, achieving 4-level programming after long-term degradation stabilization. Alternatively, at system level, short- and long-term degradation effects could be considered and modeled during network training, resulting in an overall system tolerant to such stochastic drifts [11].

In this paper we present a device-level short-term, relaxation-aware, iterative, multi-level programming technique which does not require the careful tuning of analog parameters during each device write and/or erase iteration. Fig. 2 illustrates typical hysteresis behavior during write/erase sweeps in HfO_x 1T1R devices [14]-[15]. At increasing positive voltages ($V_{BL} - V_{SL} > 0$), devices tend to transition

> REPLACE THIS LINE WITH YOUR MANUSCRIPT ID NUMBER (DOUBLE-CLICK HERE TO EDIT) <

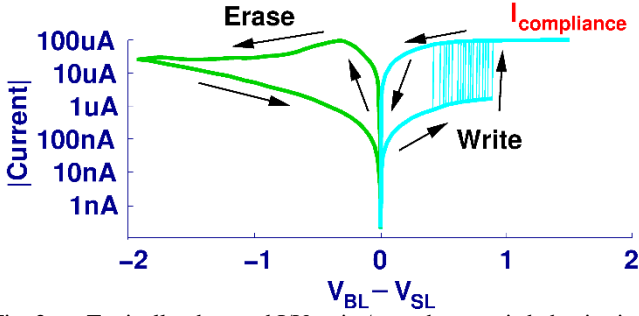


Fig. 2. Typically observed I/V write/erase hysteresis behavior in HfOx based 1T1R RRAM devices

abruptly from a low conductance state to a compliance-current-controlled higher conductance state (*Write* operation). On the other hand, with negative voltages ($V_{BL} - V_{SL} < 0$) they tend to transition smoothly from higher to lower continuous conductance levels (*Erase* operation). This observation inspired us to use only erase operations to seek the target analog programming level. Also, since we did not want to change the analog amplitude of the erasing pulses, we instead tried progressively tuning the erasing pulse width digitally. In the technique proposed here, we therefore performed *Write* operations with fixed compliance current and fixed voltage pulse width and amplitude, combined with *Erase* operations with fixed amplitude voltage pulses but variable, digitally-controlled widths. The experimental results were obtained on a 64 1T1R crossbar array fabricated in 130nm CMOS with BEOL HfOx RRAM devices. Programming without relaxation effect awareness, we obtained verified 3-level conductance 1000s after the array programming was complete, whereas programming with short-term relaxation effect awareness we obtained 4-level conductance.

Table I *Active* and *Default* mode voltages for the crossbar lines in each operation, and pulse widths for the corresponding *Active* modes.

Operation	Mode	WL	SL	BL	Pulse Width
Form	Active	1.55V	0 V	4.8 V	40 μ s
	Default	0 V	4.8 V	2.4 V	Fixed
Write	Active	1.24 V	0 V	2.4 V	100ns
	Default	0 V	2.4 V	2.4 V	Fixed
Erase	Active	4.05 V	1.07 V	0 V	CP x 10ns
	Default	0 V	0 V	2.4 V	Fixed
Read	Active	3.38 V	2.1 V	2.4 V	200 μ s
	Default	0 V	2.4 V	2.4 V	Fixed
Stand-by	-	0 V	2.4 V	2.4 V	Fixed

II. PROPOSED PROGRAMMING TECHNIQUE

Fig. 1(b) schematically represents an arbitrary-size crossbar of 1T1R devices. One column and one row of 1T1R devices is set to the *Active* mode. The other columns and rows are set to *Default* mode. Table I shows the configurations of the 1T1R devices in the crossbar for the different operations and modes, indicating the voltage values at the word lines (WL), bit lines (BL) and source lines (SL). In the *Default* mode, voltages are set to prevent any changes in the memristor states. In the *Active* modes, the corresponding lines (WL, BL, SL) are set to activate only one 1T1R target device: the one at the intersection of the horizontal and vertical *Active* lines. To

access this target device, its SL and BL lines are first changed to the corresponding *Active* values, and then, during the time shown in the *Pulse Width* column in Table I, its gate line WL is set to the *Active* voltage value. For the NMOS transistor selector in Fig. 1 and for the peripheral driving circuitry, thick oxide transistors were used that allowed for a power supply voltage of up to $V_{DD} = 4.8V$. Table I also shows a *Stand-by* state in which the SL and BL lines of all columns and rows are set to $V_{DD}/2$ while all gate lines are set to 0V. In this *Stand-by* state, there is no active line or column and no 1T1R device is targeted. The *Stand-by* state is used to transition safely between operations, avoiding possible glitches at the different lines that could unintentionally change the memory state of the memristors in the crossbar. Initially, all crossbar devices were formed with 40 μ s full V_{DD} pulses and a compliance current of about 600 μ A [3]. The write operation is always a full write, for which a write pulse of $V_{BL} - V_{SL} = 2.4V$ is applied to the target 1T1R device for 100ns while its compliance current is set to about 300 μ A by setting the gate-to-source voltage of the NMOS selector to 1.24V. For erase operations, erase pulse widths are iteratively and digitally adjusted to a multiple of 10ns (CP x 10ns, where CP is an integer). For the erase pulse amplitude $V_{SL} - V_{BL}$ and gate voltage V_{WL} a judicious compromise was reached after many trials to optimize the post-relaxation multi-level storage, resulting in the chosen values of 1.07V and 4.05V, respectively, as shown in Table I. All these voltage values were kept fixed for all devices and all programming iterations. The sequence of operations and variable-width programming iterations are controlled by an external FPGA with a 100MHz clock frequency. In future versions, we intend to use an on-chip programmable-width pulse generator with sub-ns width control [16]. Fig. 3 shows a simplified diagram of the crossbar and Active/Default selector circuits in the fabricated chip. For each Active/Default selector block, the external FPGA selects the *Active* line through the digital control word SEL_{XX} ($XX = WL, SL, \text{ or } BL$), and connects it to an external *Active* voltage bias line. The other lines are connected to an external *Default* voltage bias line. Lines $Enable_{SL}$ and $Enable_{BL}$ are normally kept ON, while line $Enable_{WL}$ is set to ON only during pulse duration. The active WL and SL lines are directly connected to external lines V_{WL}^{active} and V_{SL}^{active} , which are in turn connected by the FPGA to the pre-set bias voltages shown in Table I, depending on the operation. For a *Read* operation, the selected *Active* BL line is connected to the external opamp-based current sensing circuit shown on the right of Fig. 3. For other operations (not shown in Fig. 3), it is connected directly to bias voltage V_{BL}^{active} . During a *Read*, the selected *Active* 1T1R device current I_R is detected by sensing resistor R_{sense} . This resistor's voltage $V_R = R_{sense} \times I_R$ is measured by a DAC run by the FPGA. This way, the target 1T1R device conductance is obtained from the following equation

$$G_{1T1R} = \frac{V_R / R_{sense}}{V_{BL} - V_{SL}} \quad (1)$$

For multi-level conductance programming, the conductance range is divided into a number of intervals, each with a low value G_L and a high value G_H , inside which the conductance

> REPLACE THIS LINE WITH YOUR MANUSCRIPT ID NUMBER (DOUBLE-CLICK HERE TO EDIT) <

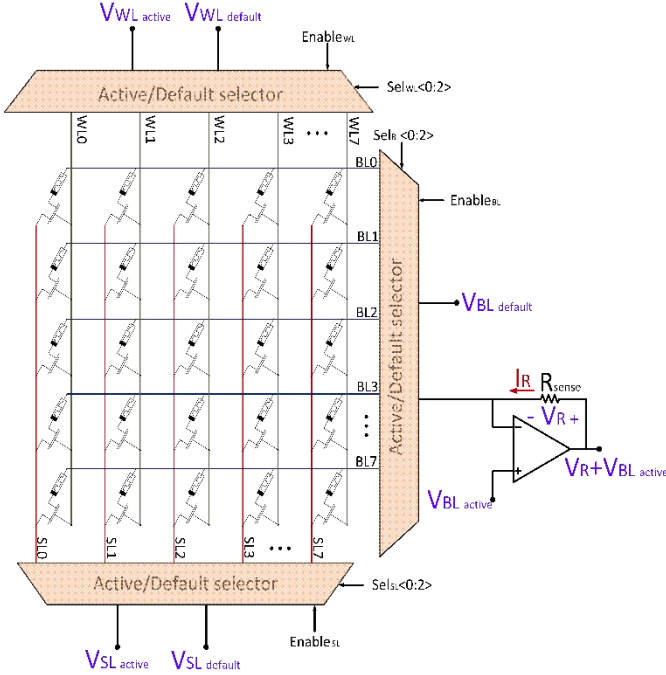


Fig. 3. Schematic architecture of the 8x8 1T1R crossbar.

will be programmed. Consecutive intervals are assigned with a conductance gap in between, to safeguard against post-programming drifts, regardless of whether a relaxation-aware technique is being used. Different ways of assigning conductance intervals were proposed in previous works. Here we use an empirical mixture of both linear and sigma-based techniques [4], as shown later in Section III.

We compared two programming techniques: one that ignores relation effects and another that considers short-term relaxation of the programmed weights:

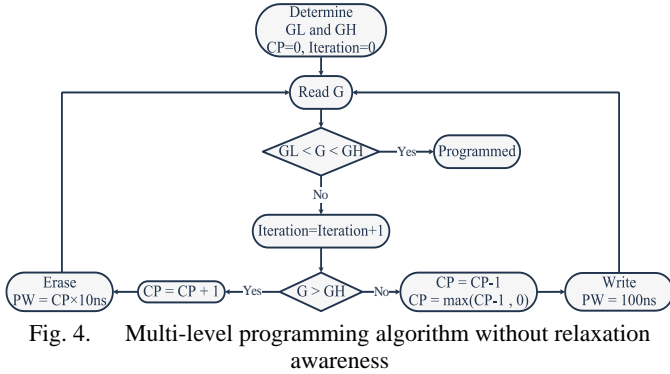


Fig. 4. Multi-level programming algorithm without relaxation awareness

A. Programming without Relaxation Awareness:

First, we programmed our crossbar array without considering relaxation effects. The algorithm used is shown in Fig. 4. Low G_L and high G_H values were set for each programming interval n , the erase pulse width coefficient CP was initialized to zero, and the target 1T1R conductance G was read. After each *Read*, if G lay inside the target programming interval, programming was finished. If it was above ($G > G_H$) we tried to lower G by strengthening the next *Erase* operation and increasing coefficient CP by one unit. We then performed the

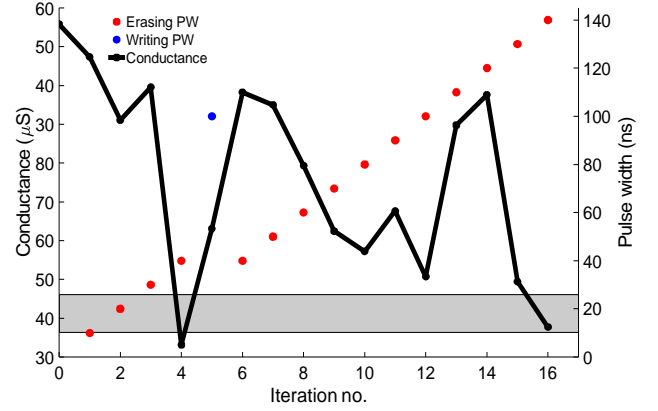


Fig. 5. Experimental illustration of a programming sequence for the algorithm in Fig. 4.

Erase operation and again read the new G . If, after a *Read*, the conductance G was below the target interval ($G < G_L$), we performed a full write with the pulse width fixed at 100ns, at the same time reducing coefficient CP by 1 in order not to strengthen the next *Erase* operation. Fig. 5 illustrates this procedure for one particular device programming sequence. The example target interval, shaded in gray, is given by $G_L = 33.2\mu S$ and $G_H = 38.08\mu S$. The horizontal axis represents the programming iteration number. The left vertical axis represents the read conductance G , and the right vertical axis represents the erase pulse width ($CP \times 10ns$, in red circles) or write pulse width (100ns, in blue squares) used immediately before the corresponding read value G . In this example, there are a total of 16 write/erase iterations until a G value inside the target interval is read. Since this conductance interval is in the lower range, most of the read conductance values are above it, resulting in the execution of *Erase* operations with increasing pulse widths (except in iteration 5, where a *Write* operation was performed). In iteration 4, an *Erase* operation was performed after which the read G was below the target interval. CP was therefore decreased, followed by a *Write* in iteration 5. In this iteration the newly read G value was above the interval, thus increasing CP again and providing an *Erase* pulse for iteration 6 of the same width as the latest *Erase* pulse (iteration 4). It is interesting to observe the stochastic nature of the different *Erase* pulses, as they produced both increments and decrements in conductance. Although there did not appear to be any clear correlation between pulse width and conductance, such correlation did in fact exist, as described in Section III.

B. Programming with Short-Term Relaxation Awareness:

It is well known that sub-micron-size HfOx 1T1R devices suffer from short- and long-term stochastic degradation effects, which are more pronounced a) when trying to program multi-level conductance levels, and b) during the first few seconds after programming [4],[11]. To compensate for this, Esmanhotto et al. [5] proposed waiting for a time Δt after each programming before doing any *Read* operations, concluding that with $\Delta t = 5s$ four distinct conductance levels could safely be programmed in a crossbar array. Inspired by this mitigation technique, here we propose a slightly modified alternative.

> REPLACE THIS LINE WITH YOUR MANUSCRIPT ID NUMBER (DOUBLE-CLICK HERE TO EDIT) <

obtain distinguishable 4-level conductance intervals. In Fig. 5 we saw that the programming process had a high degree of stochasticity. To find out whether any correlation exists between the target states and the final *Erase* pulse width, Fig. 10 shows, for each 1T1R device and each initial target state defined in Table II ($n = 0$ to 7), the final *Erase* pulse width used for all programming iterations and for both programming algorithms. A strong correlation can be seen: the average final *Erase* pulse width increases as target conductance values decrease. 0 shows, for each target state, the average number of programming iterations used (\bar{n}_{iter}) and the average final *Erase* pulse width (AFEPW) for each programming cycle and for both algorithms. For \bar{n}_{iter} there is no clear correlation with the target state. The $\Delta\bar{n}_{iter}$ column represents the average number of iterations the algorithm in Fig. 6 went through the Δt branch. Here too, there is a clear correlation: as the conductance increases, the algorithm requires more times to go through the waiting branch. An iteration without waiting takes about 120ms, mainly due to settling delays when changing operation modes.

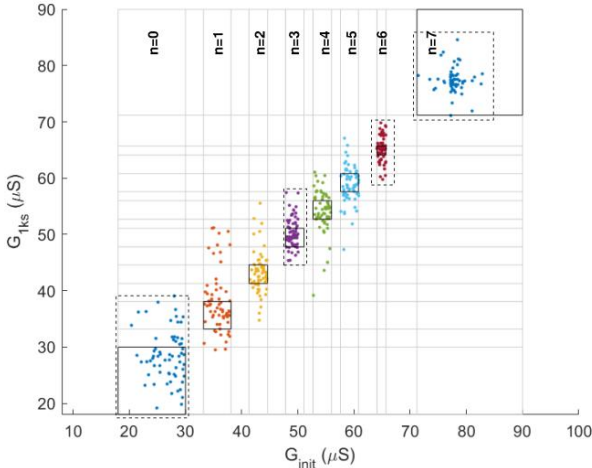


Fig. 9. Final conductance values, measured 1ks after programming when using the slower short-term relaxation-aware programming technique in Fig. 6.

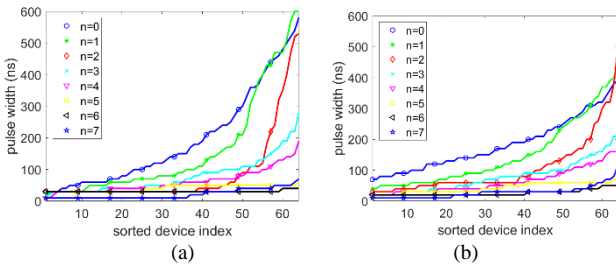


Fig. 10. The graph shows the final erase pulse width used for each of the 64 1T1R devices and for each programmed state. The 1T1R indexes are sorted by increased pulse width for each state. (a) Results for the faster algorithm in Fig. 4. (b) Results for the slower short-term relaxation-aware algorithm in Fig. 6.

V. CONCLUSIONS

In this paper we propose a fully digital short-term relaxation-aware erase pulse width multi-level programming technique for HfOx-based 1T1R crossbars. We report experimental

measurements on a 64-device crossbar fabricated in CEA-LETI monolithic CMOS+RRAM 130nm technology. The experimental results demonstrate that it is possible to obtain 4-level (2-bit) programming, verified 1000 seconds after full array programming.

Average iterations and final Erase pulse widths

State#	No waiting (Fig. 4)		$\Delta t = 5s$ (Fig. 6)		$\Delta\bar{n}_{iter}$
	\bar{n}_{iter}	AFEPW (ns)	\bar{n}_{iter}	AFEPW (ns)	
n=0	19	184	21	193	2
n=1	10	150	13	161	3
n=2	9	105	12	86.6	3
n=3	15	78.0	21	78.8	6
n=4	14	63.3	20	61.6	6
n=5	13	42.7	24	39.1	11
n=6	11	26.1	16	30.8	5
n=7	3	27.8	26	22.2	23

ACKNOWLEDGEMENTS

This work was partly funded by EU grants 871501, 824164, 899559, 101070908, and National grant PID2019-105556GB-C31 (with support from the European Regional Development Fund).

REFERENCES

- [1] D. Burger, et al. "Memory bandwidth limitations of future microprocessors," *Int. Symp. on Comp. Arch.*, May 1996.
- [2] T. M. Bartol Jr, et al. Nanoconnectomic upper bound on the variability of synaptic plasticity. *Elife*, 4: e10778, 2015.
- [3] A. Grossi et al., "Experimental Investigation of 4-kb RRAM Arrays Programming Conditions Suitable for TCAM," *IEEE Trans. on Very Large Scale Integ. (VLSI) Syst.*, vol. 26, no. 12, pp. 2599-2607, Dec. 2018
- [4] E. Esmanhotto, et al. "High-density 3D monolithically integrated multiple 1T1R multi-level-cell for neural networks." *2020 IEEE Int. Electron Devices Meeting (IEDM)*.
- [5] E. Esmanhotto, et al. "Experimental demonstration of Single-Level and Multi-Level-Cell RRAM-based In-Memory Computing with up to 16 parallel operations." *2022 IEEE Int. Reliability Physics Symp. (IRPS)*.
- [6] M. Payvand, et al. "Analog Weight Updates with Compliance Current Modulation of Binary ReRAMs for On-Chip Learning," *2020 IEEE Int. Symp. on Cir. and Syst. (ISCAS)*, 2020, pp. 1-5.
- [7] P. Yao et al., "Fully hardware-implemented memristor convolutional neural network," *Nature*, vol. 577, no. 7792, pp. 641-646, 2020.
- [8] C. Li et al., "Analogue signal and image processing with large memristor crossbars," *Nature Electron.*, vol. 1, no. 1, pp. 52-59, 2018.
- [9] E. Pérez, et al., "Toward reliable multi-level operation in RRAM arrays: Improving post-algorithm stability and assessing endurance/data retention," *IEEE J. Electron Devices Soc.*, vol. 7, pp. 740-747, Jul. 2019.
- [10] W. Wan, et al. "A compute-in-memory chip based on resistive random-access memory." *Nature* 608.7923 (2022): 504-512.
- [11] Y. Xi et al., "Impact and Quantization of Short-Term Relaxation effect in Analog RRAM," *2020 4th IEEE Electron Devices Technology & Manufacturing Conference (EDTM)*, 2020, pp. 1-4.
- [12] E. R. Hsieh et al., "High-density multiple bits-per-cell 1T4R RRAM array with gradual SET/RESET and its effectiveness for deep learning," *IEDM Tech. Dig.*, Dec. 2019, pp. 843-846.
- [13] E. R. Hsieh et al., "Four-bits-per-memory one-transistor-and-eight resistive-random-access-memory (1T8R) array," *IEEE Electron Device Lett.*, vol. 42, no. 3, pp. 335-338, Mar. 2021.
- [14] Le, Binh Q., et al. "Resistive RAM with multiple bits per cell: Array-level demonstration of 3 bits per cell." *IEEE Trans. on Elect. Dev.* 66.1 (2018): 641-646.
- [15] C. Giovinazzo, et al. "Analog Control of Retainable Resistance Multistates in HfO2 Resistive-Switching Random Access Memories (ReRAMs)." *ACS Applied Electronic Materials* 1.6 (2019): 900-909.
- [16] H. Erfanijazi, T. Serrano-Gotarredona and B. Linares-Barranco, "Novel programmable single pulse generator for producing pulse widths in different time scales," *2021 Int. Conf. on Content-Based Multimedia Indexing (CBMI)*, 2021, pp. 1-6.